*Small Structures*

small structures

www.small-structures.com

RESEARCH ARTICLE OPEN ACCESS

# Bioinspired Fabric Ligament with Tunable Stiffness for Reproducing 3D Lumbar Spine Kinematics

Guangsheng Song[1,2] | Weilong Jin[1] | Guanghui Li[1] | Yushan Sun[1] | Jianan Wu[1] | Hounan Song[1] | Yuyang Wei[3] | Kaize Wang[1] | Zhende Jiang[4] | Zhihui Qian[1,5] | Lei Ren[1,5,6] | Luquan Ren[1,2]

[1]Key Laboratory of Bionic Engineering, Ministry of Education, Jilin University, Changchun, China | [2]Weihai Institute for Bionics, Jilin University, Weihai, China | [3]Department of Engineering Science, University of Oxford, Oxford, UK | [4]Orthopaedic Medical Center, The Second Hospital of Jilin University, Jilin University, Changchun, China | [5]Institute of Structured and Architected Materials, Liaoning Academy of Materials, Shenyang, China | [6]Department of Mechanical, Aerospace and Civil Engineering, University of Manchester, Manchester, UK

**Correspondence:** Zhihui Qian (zhqian@jlu.edu.cn)

**Received:** 6 November 2025 | **Revised:** 10 January 2026 | **Accepted:** 12 January 2026

**Keywords:** bioinspired design | bioinspired lumbar spine system | multimaterial additive manufacturing | polymeric fabric architecture | tunable stiffness

## ABSTRACT

Lumbar spine ligaments play a critical role in maintaining spine joint stability and structural integrity within segmental biomechanics. However, most existing lumbar spine models and simulators neglect ligament contributions, leading to incomplete or potentially overestimated evaluations of spinal implant performance. Herein, we introduce bioinspired fabric ligaments (BFLs), designed to emulate the hierarchical structure and material properties of natural spine ligaments. By tailoring fabric architecture, strand number, and yarn count, BFLs successfully reproduce the nonlinear force–displacement behavior and tunable stiffness characteristics of natural spine ligaments. Integrating BFLs with three-dimensional (3D) printed bioinspired vertebrae and intervertebral disc (IVD), we develop a bioinspired lumbar spine system (BLSS). The experimental results demonstrate that the developed BLSS not only restricts the excessive motion of ligament-deficient models but also replicates physiologically relevant 3D lumbar kinematics. This work establishes a versatile paradigm for ligament-mimetic design, offering a reliable platform for intervertebral implants evaluation and new opportunities for personalized spinal implants optimization.

## 1 | Introduction

Lumbar degenerative disc disease has become a major global health concern, leading to substantial healthcare expenditures and imposing a considerable economic burden on patients and their families [1, 2]. Due to its high incidence, multifactorial etiology, and diverse clinical manifestations, selecting the appropriate treatment strategies remains a complex challenge. Common and effective surgical strategies involve the use of lumbar interbody fusion (LIF) cages [3] or total disc replacement (LTDR) devices [4]. These procedures address structural pathologies, significantly alleviate pain, and restore lumbar spine biofunction. Consequently, the functional properties of these implants are critical determinants of their clinical outcomes.

To evaluate the biomechanical performance of spinal implants, several representative testing approaches have been identified, including biological specimens [5, 6], finite element analysis (FEA) [7, 8], and spinal simulators [9–11]. Biological specimens, such as human cadaveric and animal models, enable realistic simulation of spinal motion and mechanical behavior under physiological loading conditions. Since biological specimens largely preserve the biomechanical properties of native tissues, their data hold high empirical value and provide reliable evidence for biomechanical analysis [12, 13]. However, these approaches come with limitations, including strict ethical constraints, high experimental costs, challenges in specimen acquisition, and the absence of a true physiological environment. Moreover, inherent differences between animals and humans, as well as variability between specimens, limit the generalizability of experimental findings [13]. FEA has become another widely adopted approach to construct spine models [14], owing to its ability to reproduce complex anatomical geometries and heterogeneous, anisotropic

material properties. FEA offers a cost-effective and noninvasive tool that allows systematic variation of parameters, prediction of extreme loading conditions, and virtual testing of implants or surgical techniques. These advantages make FEA an indispensable method for exploring spinal biomechanics and optimizing clinical interventions. Nevertheless, the predictive accuracy is highly dependent on the reliability of input parameters and modeling assumptions. The nonlinear and viscoelastic properties of spinal tissues are difficult to fully characterize, and simplified boundary conditions, contact definitions, and loading applications may not fully capture physiological realities [15]. Furthermore, the lack of adequate experimental validation and the challenges in accounting for interindividual anatomical variability further limit the translational potential of current models [16]. While FEA provides valuable insights into spinal biomechanics and implant design, its results should be interpreted with caution and supported by experimental or clinical data. To address these limitations, spinal simulators (e.g., spine testing machines and synthetic spine models) have been developed in accordance with ASTM/ISO standards [9, 10]. These simulators enable the basic evaluation of intervertebral implants. However, their loading modes are often oversimplified and fail to accurately replicate physiological spinal motion [17]. More critically, they commonly neglect the structural and functional role of ligaments, leading to exaggerated ranges of motion (ROM) and reducing the fidelity of biomechanical assessments. This results in substantial deviations from physiological reality and undermines the reliability of experimental results [10, 18]. Thus, integrating ligamentous constraints into the spinal testing systems is essential to achieve high biomechanical fidelity and enhance their clinical relevance.

The human lumbar spine is a highly complex biomechanical system, in which the natural intervertebral discs (IVD), facet joints, and surrounding ligaments work synergistically to maintain stability while allowing appropriate physiological mobility [19, 20]. Among these structures, natural ligaments play a critical role in connecting bones, constraining excessive motion, distributing loads, and preventing injury [21–23]. Natural ligaments are hierarchically composed of subfascicular bundles of collagen fibers, which are further organized in bundles of collagen fibrils [21, 24]. Mimicking these structural features using engineered materials offers a promising strategy for developing bioinspired ligament substitutes with tunable stiffness to reproduce the kinematics of the lumbar spine. In particular, fabric-based structures have demonstrated superior flexibility, continuous personal cooling [25], durability [26], strain programmability [27], fatigue resistance [28], bio-motion energy harvesting [29], and anisotropic response [30], aligning closely with the functional requirements of spinal ligaments [31]. Herein, we propose bioinspired fabric ligaments (BFLs) for the lumbar spine, which possess tunable stiffness properties that closely mimic those of natural ligaments. When integrated into a bioinspired lumbar spine system (BLSS), the developed BFLs are expected to provide physiologically relevant motion constraints and ROM, thereby enhancing the fidelity of biomechanical testing and offering new insights into musculoskeletal tissue engineering.

## 2 | Results and Discussion

### 2.1 | Design Principle of BFLs

The functional spinal unit (FSU) is the fundamental structural component of the human lumbar spine, typically consisting of upper and lower vertebrae, natural IVD, and surrounding ligaments (Figure 1). Natural ligaments are essential connective tissue complexes and possess nonlinear mechanical property and tunable mechanics [32]. The mechanical properties arise from the hierarchical structure of natural ligaments, enabling adaptation across spinal levels and loading modes. At the microscale, the collagen fiber diameter, orientation, arrangement, and cross-link density control stiffness evolution. At the macroscale, variations in fiber bundle architecture, ligament morphology, allow different ligaments—and even the same ligament at different spinal levels—to exhibit tunable stiffness and nonlinear property. Consequently, the nonlinear mechanical property and tunable stiffness are achieved by hierarchical structure. To connecting adjacent vertebrae, the ligaments, together with the surrounding spinal muscles, enable controlled physiological movement and maintain fixed postural positions. They also play a critical role in constraining excessive intervertebral joint motion, enhancing joint stability, and protecting the spinal cord [19]. The FSU is mainly composed of seven distinct ligaments, each with unique morphology, dimensions, attachment sites, and functional characteristics. These ligaments include the anterior longitudinal ligament (ALL), the posterior longitudinal ligament (PLL), the intertransverse ligament (ITL), the interspinal ligament (ISL), the supraspinal ligament (SSL), the ligamentum flavum (LF), and the capsular ligament (CL). Each ligament serves a specific biomechanical function and contributes to the overall mobility and stability of the lumbar spine.

Fabric structures can effectively mimic the hierarchical structure and nonlinear mechanical properties of natural ligaments through the controllable number of fiber strands and layers. By integrating biomimetic principles with fabric technology, BFLs with tunable stiffness properties can be achieved. Bioinspired designs, including knit, single woven, and double woven structures, were proposed. This approach not only allows precise control over the spatial arrangement of fibers but also enables tuning of the mechanical properties by adjusting structural parameters such as the number of strands and yarns. Ultimately, this results in BFLs with biomechanical characteristics that closely resemble those of natural ligaments. BFLs were fabricated using polyethylene (PE) wire [33], and uniaxial tensile tests were carried out using a universal testing machine (UTM5504, SUNS, China) in Figure S1. The results indicated that different fabric structures could effectively control the stiffness of BFLs. The double woven structure exhibited the highest stiffness, followed by the knitted structure with intermediate stiffness and the single woven structure, which had the lowest stiffness. Based on the anatomical parameters, morphological features, and tensile strength of each natural ligament, appropriate fabric patterns were selected to fabricate BFLs.

### 2.2 | BFLs with Tunable Property for the BLSS Application

To elucidate the influence of strand number on the structural stiffness in knit, single woven, and double woven structures, mechanical responses were quantitatively evaluated (Figure 2). BFLs with varying strand counts were fabricated (Figure 2a) and subjected to uniaxial tensile testing based on the three proposed design approaches. BFLs stiffness exhibited a significant positive correlation with strand number (Figure 2b–d). Increasing the strand numbers from 4 to 12 results in a steepening of the

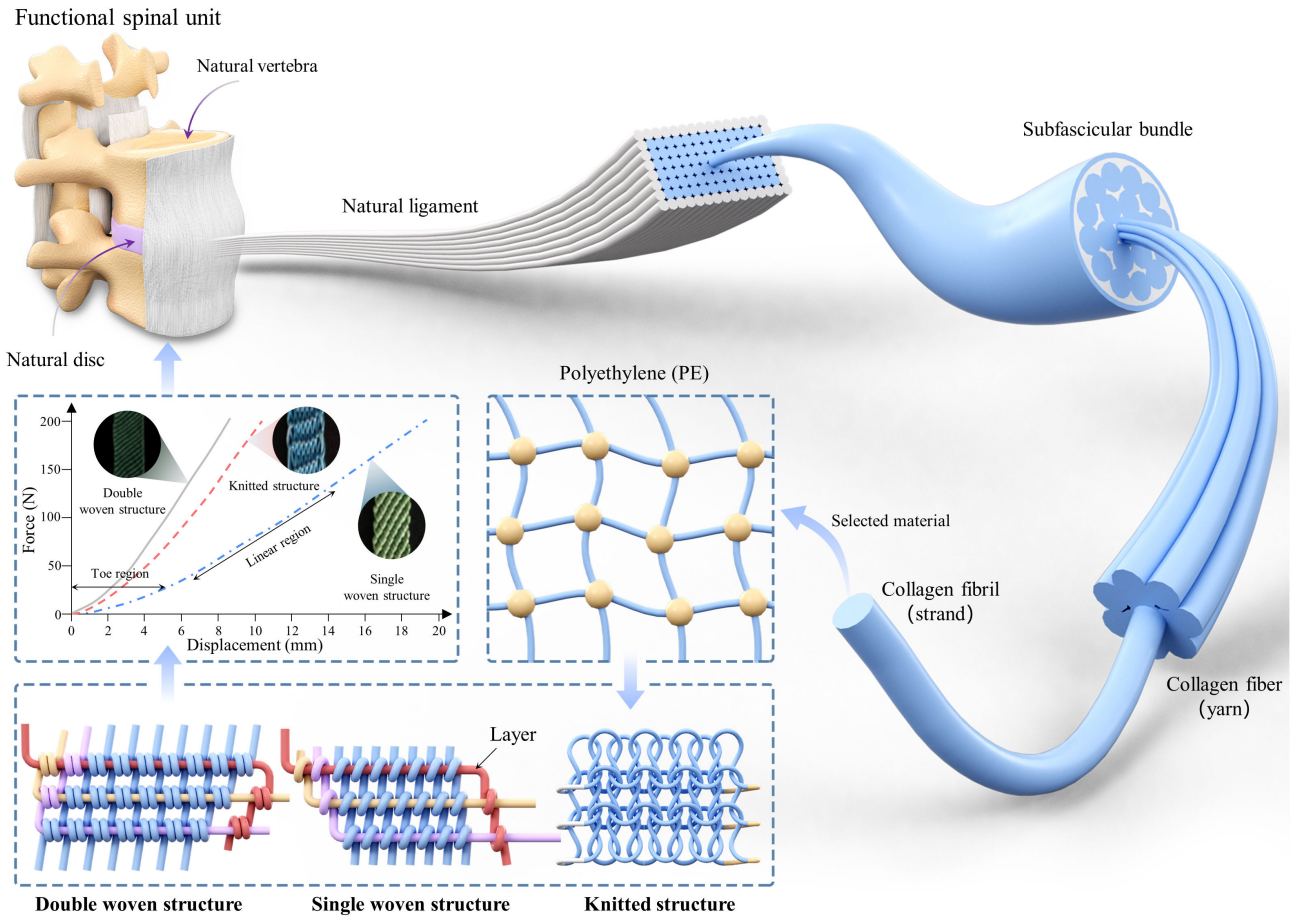


**FIGURE 1** | Design principle of BFLs based on the hierarchical structure of natural ligament. Natural ligament is hierarchically organized, consisting of subfascicular bundles composed of collagen fibers, which are assemblies of collagen fibrils. Drawing inspiration from this hierarchical structure, BFLs are designed to reproduce the nonlinear mechanical behavior characteristic of natural ligaments.

force–displacement curve in the identical structural configurations, revealing a stiffness enhancement with increasing strand number. These findings indicated that BFLs stiffness could be effectively tuned by selecting the appropriate number of strands, thereby providing a critical strategy and rationale for achieving tunable stiffness in the engineering design of BFLs.

Building on this, the influence of the number of yarns on BFLs stiffness was further investigated (Figure 3). The tensile testing process and representative specimens are shown in Figure 3a,b, respectively. The yarn count provides a moderate tuning parameter for controlling BFL stiffness (Figure 3c). For example, the partial stiffness of BFLs is illustrated (Figure 3d). These quantitative results indicated that the overall stiffness of BFLs increased linearly with the number of yarns at a fixed strand number. Similar trends were observed across different strand counts under the identical structural conditions. Taken together, these results indicated that the number of yarns provided a modest and nonlinear tuning effect on the stiffness of the BFLs. The mechanical behavior is probably attributable to the enlarged cross-sectional load-bearing area and enhanced interfiber interactions associated with a greater number of yarns. By quantitatively analyzing the relationships among strand numbers, yarn counts, and stiffness coefficients, this study provides experimental evidence supporting the feasibility of tuning the stiffness in BFLs, offering valuable guidance for their structural optimization.

According to the design principles described above, individual BFLs were developed to replicate the functional characteristics and morphological features of natural ligaments for reconstructing the BLSS in Figure 4. The individual sample is shown in Figure 4a, and the detailed parameters of the fabricated BFLs are summarized in Table 1. The mechanical property of each BFL was validated compared to the reported data in previous literature (Figure 4b). The results indicated that the developed BFLs exhibited J-shaped force–displacement behavior and stiffness values comparable to those of natural ligaments in toe region (Figure S2), which was consistent with the results reported in the literature [34–36]. However, the deviations were generated in the linear region. These deviations might be further reduced by refined structural configuration and parameter tuning. To accurately replicate specific spinal morphology and biomechanics, the personalized bioinspired vertebrae and IVDs with complex anatomical architectures were fabricated by additive manufacturing technology [37, 38]. Furthermore, three-dimensional (3D) models of natural L3–L5 vertebrae were reconstructed from lumbar computed tomography (CT) images (Figure S3), the geometric model were shown and bioinspired vertebrae was fabricated via photopolymerization-based 3D printing (Figure S4), and the detailed parameters were listed in Table S1. Based on the function–structure characteristics of natural IVD [39, 40], bioinspired IVD in different segments was designed (Figure S5 and

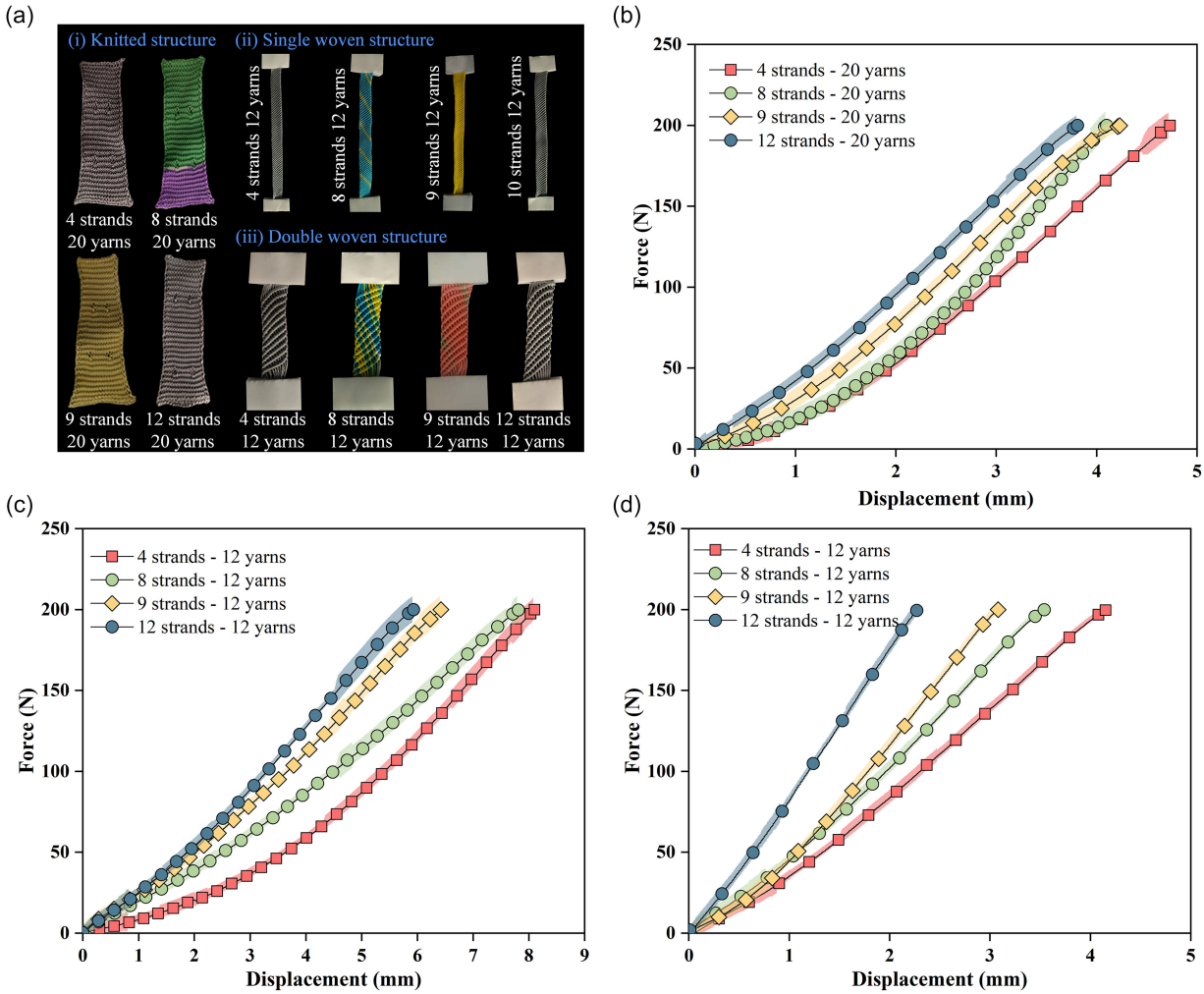


**FIGURE 2** | The effect of knit, single woven, and double woven structures under varying strand numbers with a fixed number of yarns. (a) The fabricated BFL samples. (b) Tensile testing results of the knitted structure with varying strand numbers at fixed 20 yarns. (c) Tensile testing results of the single woven structure with varying strand numbers at fixed 12 yarns. (d) Tensile testing results of the double woven structure with varying strand numbers at fixed 12 yarns.

Figure S6) and the relevant structural parameters was individually shown in Table S2 and Table S3. Bioinspired IVD samples were eventually fabricated using multimaterial 3D printing. In addition, the upper and lower fixation blocks were manufactured from polylactic acid (PLA) using fused deposition modeling technology (Figure S7). By integrating the developed BFLs, the BLSS was assembled (Figure 4c).

## 2.3 | The Integrated BLSS for Reproducing Physiological Lumbar Kinematics

While individual BFL provides critical insights into structure–property relationships, they cannot fully reproduce the coupled motion and constraints function of the lumbar spine. By embedding multiple BFLs within a segmental vertebral framework, the developed system reproduces physiologically relevant spinal kinematics and stability, thereby revealing the coupling relationship between BFLs and whole-spine kinematics. However, assembly strategies (including the sequence of component integration) play a critical role in determining the transmission of mechanical errors, stress distribution, and constraints on the system's degrees of freedom, all of which directly influence the stability and motion precision of the mechanical system [41, 42]. We investigated the effect of different assembly methods on the biomechanical performance of the BLSS (Figure 5), considering three different assembly strategies (Method I, Method II, and Method III) (Figure 5a). As a baseline, an assembly without BFLs (Method IV) was also evaluated. Using a previously established testing platform equipped with a KUKA robotic arm under controlled experimental conditions (Figure 5b) in Figure S7 [17], we quantified the ROM for the developed BLSS by mimicking the 3D kinematic patterns of a natural spine. These static kinematic patterns in anatomical planes, including extension/flexion (Movie S1), lateral bending (Movie S2), and axial rotation (Movie S3), are shown in Figure 5c.

As illustrated in Figure 5d, the experimental results of the assembly Method I indicate that the designed model can reproduce the nonlinear variable-stiffness behavior of the natural lumbar spine. However, the motion patterns exhibited deviations from the physiological data, particularly with pronounced lateral bending. Moreover, under relatively high applied moments, a sudden increase in displacement was observed. These results suggested that

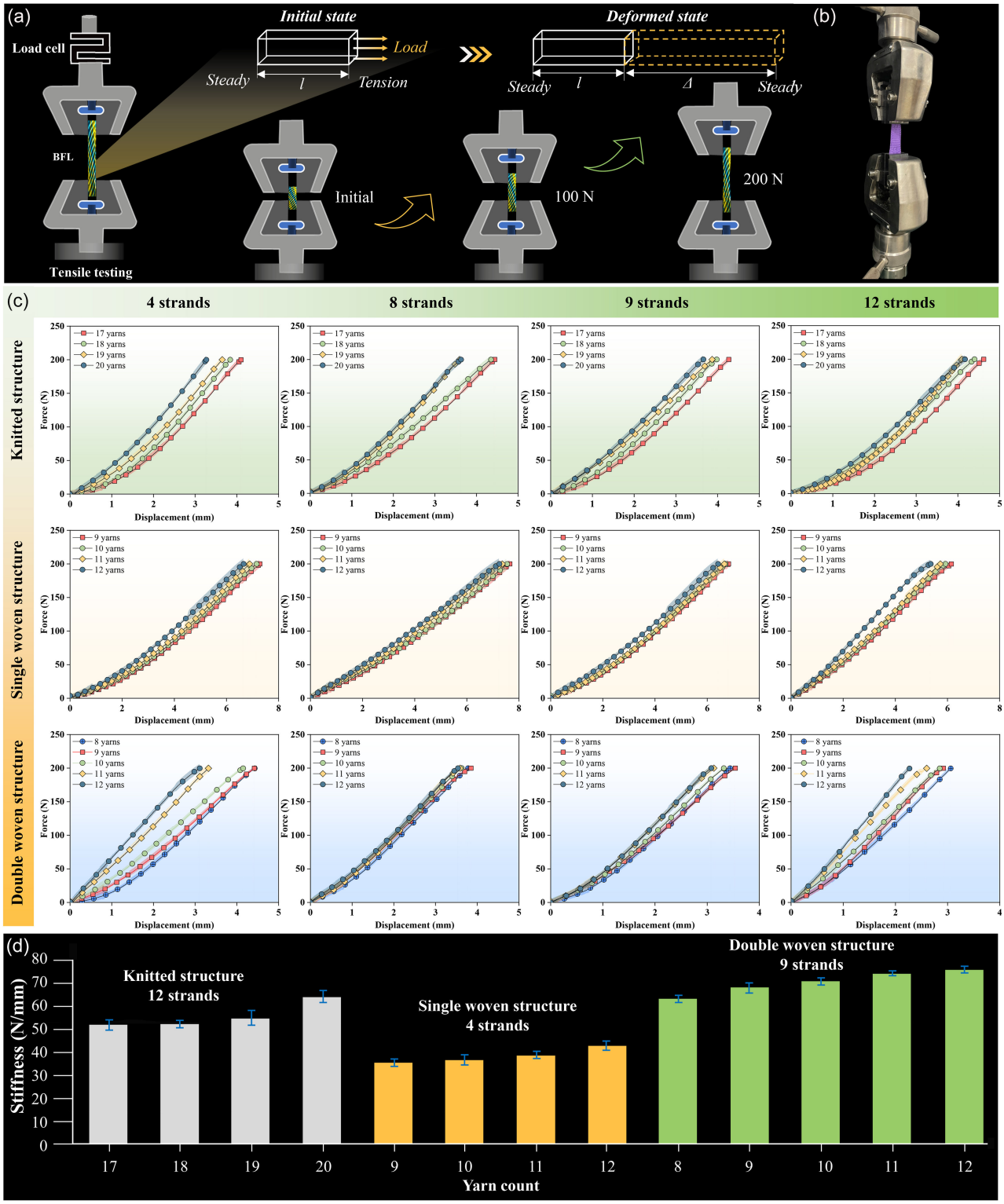


**FIGURE 3** | The effect of knit, single woven, and double woven structures under varying yarn numbers with a fixed number of strands. (a) Demonstration of the tensile testing process. (b) Tensile testing of BFLs. (c) The effect of yarn counts on stiffness in knitted, single woven, and double woven structures at fixed strand numbers. (d) Part of the relationship between stiffness and yarn number for BFLs.

the posterior BFLs, including the B-PLL, B-LF, and B-ISL, could not achieve sufficient preload because the bioinspired IVD was first installed, before the BFLs. The experimental results for assembly Method II demonstrated better reproduction of the nonlinear variable-stiffness behavior of natural IVD compared to Method I. However, because B-PLL and B-LF were first installed, the ROM still deviated from physiological behavior. During testing, the flexion movement caused the ligaments to stretch, resulting in fluctuations in the measured flexion values. Additionally, the B-ITL, located laterally, had minimal impact on lateral bending motions, and

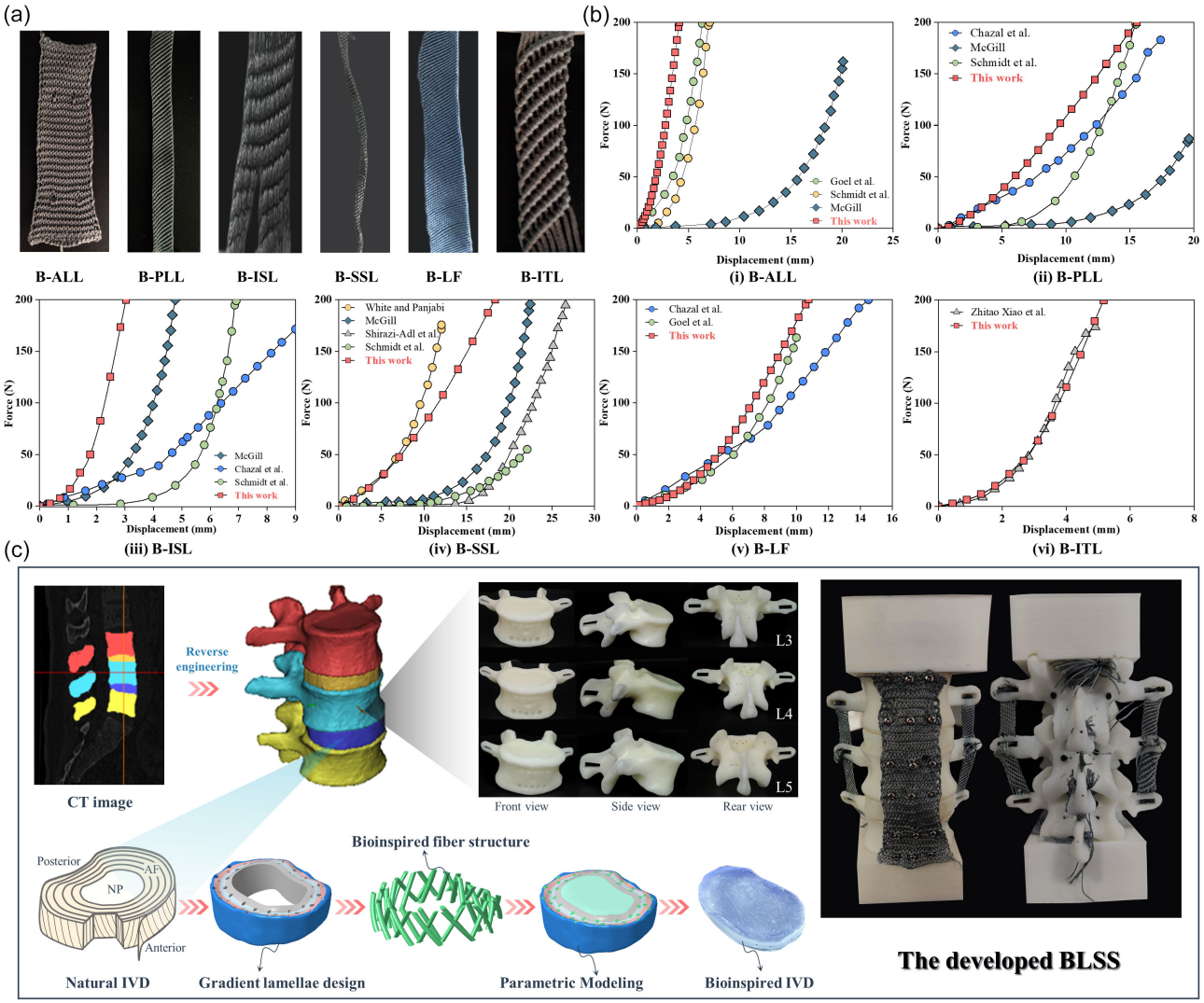


**FIGURE 4** | Developing BFLs for the integrated BLSS. (a) Individual BFLs. (b) Force–displacement curves of BFLs compared to reported cadaveric data [34, 35]. (i) Force–displacement response of B-ALL in comparison with the cadaveric data. (ii) Force–displacement response of B-PLL in comparison with the cadaveric data. (iii) Force–displacement response of B-ISL in comparison with the cadaveric data. (iv) Force–displacement response of B-SSL in comparison with the cadaveric data. (v) Force–displacement response of B-LF in comparison with the cadaveric data. (vi) Force–displacement response of B-ITL in comparison with the cadaveric data. (c) The BLSS integrating BFLs, bioinspired vertebrae, and bioinspired IVDs. The integrated BLSS for reproducing 3D lumbar spine motions.

**TABLE 1** | The developed BFLs parameter.

| Type | Structure | Parameter | | |
|---|---|---|---|---|
| | | Strand | Yarn | Layer |
| Bioinspired ALL (B-ALL) | Knit | 12 | 20 | 30 |
| Bioinspired PLL (B-PLL) | Single woven | 12 | 12 | 56 |
| Bioinspired ISL (B-ISL) | Single woven | 9 | 24 | 50 |
| Bioinspired SSL (B-SSL) | Double woven | 12 | 10 | 5 |
| Bioinspired LF (B-LF) | Single woven | 4 | 4 | 36 |
| Bioinspired ITL (B-ITL) | Double woven | 12 | 10 | 7 |

the pretension effect did not reach the intended level. Assembly Method III, which prioritized the installation of all BFLs prior to the bioinspired IVD, more accurately reproduced the nonlinear variable-stiffness behavior observed in physiological human lumbar spine motion, aligning with human motion characteristics. The experimental results for assembly Method III illustrated that the

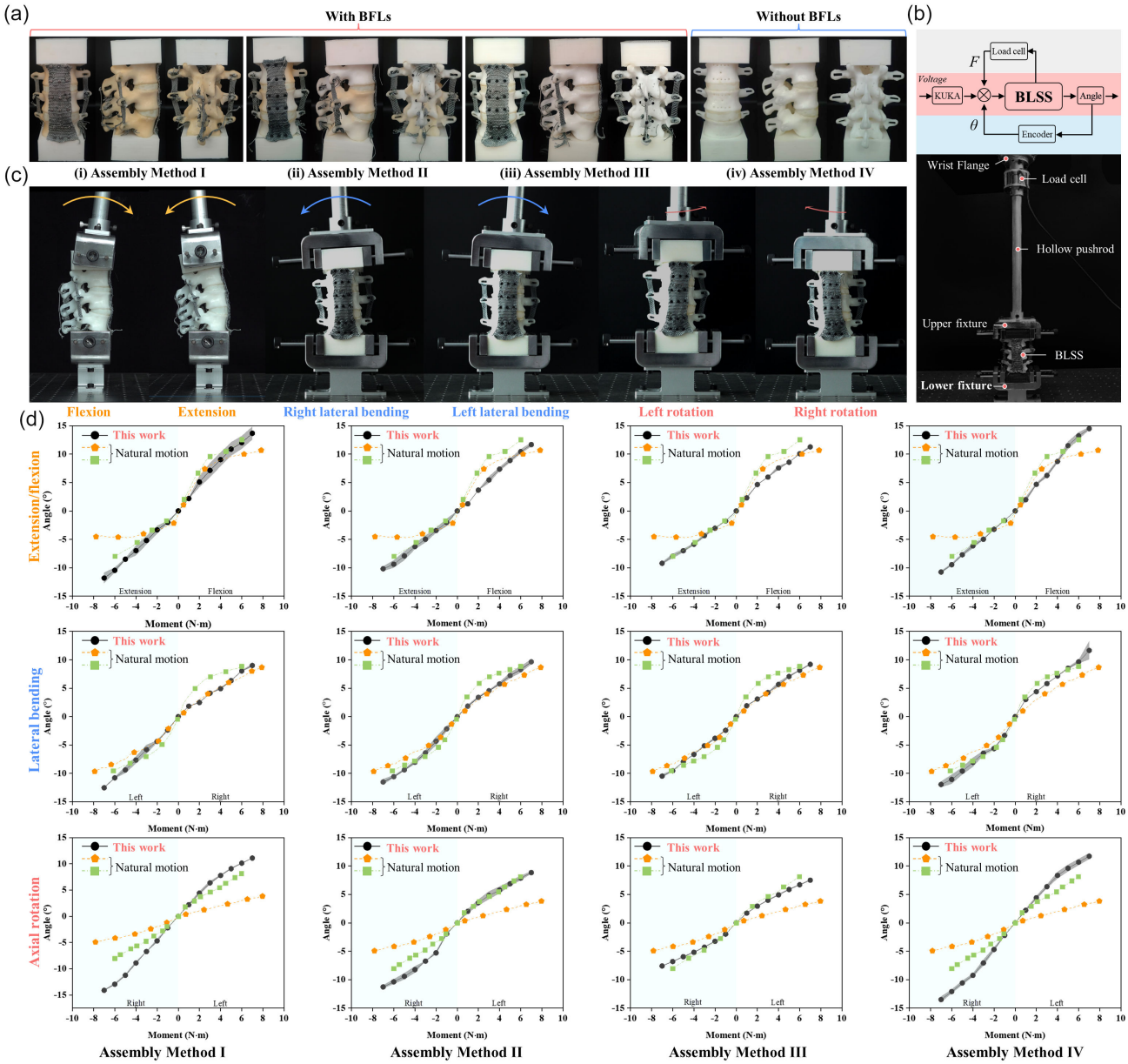


**FIGURE 5** | The 3D kinematic performance of the integrated BLSS. (a) Various assembly methods. Assembly Method I: the bioinspired IVD and the three-segment bioinspired vertebra were first assembled and fixed using super glue (epoxy resin adhesive, UHU, Germany), followed by the installation of the BFL. Assembly Method II: the B-PLL, B-LF, and B-ALL were initially assembled with the three segments of bioinspired vertebra. The bioinspired IVD was then glued between the vertebrae, followed by the B-ITL, B-ISL, and B-SSL. Assembly Method III: each BFL and the three segments of bioinspired vertebrae were assembled first, followed by the integration of the bioinspired IVD. Assembly Method IV: the bioinspired IVD and the three-segment bioinspired vertebrae were assembled without BFLs. (b) In vitro testing device. (c) Simulation of the 3D motion characteristics of the human lumbar spine. (d) ROM results and comparison with reported cadaver data [43–45].

installation of the B-ITL primarily influenced lateral bending and axial rotation. Following the installation of the bioinspired IVD, the disc distance increased, allowing the B-ITL to straighten and achieve the required pretension. Similarly, installing the B-ALL first influenced the extension motion, and after the disc was installed, the intervertebral spacing increased, straightening the ligament to meet its pretension requirements. Therefore, assembly Method III was ultimately selected as the preferred strategy for assembling the BLSS. In assembly Method IV, under a 7.5 N/m moment, the flexion angle reached approximately 11°, exceeding the normal physiological range of the human lumbar spine, in agreement with the previous work [17]. The excessive ROM observed with bioinspired IVD is attributable to the absence of BFLs, which compromises the ability of the system to reproduce the intended motion under the applied moment. These experiment data highlight the critical role of BFLs in constraining excessive lumbar extension. In addition, the ROM comparison before and after fatigue testing demonstrated that BLSS possessed long-term stable mechanical properties (Figure S9). Consequently, the developed BLSS provides a more accurate reproduction of 3D physiological motions and improves biomechanical fidelity compared to current ligament-deficient or ligament-free models [11, 17].

From the above comparative analysis, it was evident that the experimental results exhibited both consistencies and discrepancies when compared to the biomechanical data of the intact human cadaveric specimens [45–47]. These discrepancies are likely attributable to the omission of natural CL in this study, as its irregular geometry and pronounced intersegmental variability make accurate reconstruction with artificial structures technically challenging. However, the omission of natural CL leads to increased intersegmental ROM and reduces rotational stiffness, especially in flexion/extension and axial motions. Consequently, the neglecting the CL is to overestimate the segmental ROM in flexion/extension and axial motions for the present BLSS. In future work, the biomechanical contribution of natural CL will be explicitly incorporated to further improve the accuracy and physiological relevance of the developed BLSS.

Although certain deviations in the ROM were existed during the flexion phase, the remaining motion patterns fall within the ranges reported in the reported literature. This finding demonstrated that the introduction of the proposed BFL improved the physiological fidelity of spinal motion reproduction compared to a configuration without BFLs due to the developed BFLs with nonlinearity and tunable stiffness. Recently, several mechanical metamaterials by additive manufacturing technology, such as honeycomb and auxetic metamaterial, exhibit nonlinear and tunable mechanical responses through geometry-controlled deformation mechanisms. While these designs can achieve pronounced nonlinearity and stiffness modulation, their mechanical responses are primarily governed by discrete geometric instabilities and unit deformation modes, which lead to abrupt stiffness transitions, strong loading-direction dependence, and localized stress concentrations [48]. In contrast, the developed BFLs originate from fundamentally different fiber structure configuration. This fiber-dominated hierarchical architecture enables a smooth, continuous J-shaped stress–strain response and tunable stiffness, allowing the ligament to remain compliant at low strains to accommodate physiological joint motion, while gradually increasing stiffness under higher strains to ensure joint stability. Overall, the developed BLSS provides a robust platform for evaluating the mechanical performance of intervertebral implants and offers a new tool for personalized design optimization.

## 3 | Conclusion

In this work, a biomimetic lumbar ligament design and fabrication approach based on fabric technology was proposed. By optimizing the fabric structure, strand number, and yarns count, the mechanical properties of BFLs can be tuned to ensure that passive joint constraints during lumbar segment motion simulation more closely replicate physiological conditions. To date, few studies have reported a BLSS that integrates biomimetic principles, fabric technology, and 3D printing. Based on this, the BLSS was developed to reproduce the physiological 3D motion characteristics of lumbar spinal segments. 3D models of natural vertebrae, IVD, and ligaments are reconstructed based on the CT image, providing the anatomical basis for customized design. These models provide the geometric framework for the BLSS, enabling precise mapping of implant surfaces and internal structures to the patient's spinal morphology. Personalized and parameterized design is further achieved by modulating ligament architecture to replicate the biomechanical behavior of the natural spine. Scaling across different spinal levels is realized by adjusting the BLSS geometric dimensions, segment-specific stiffness, and ligament parameters to match the anatomical size and functional demands of each level, ensuring consistent physiological ROM. Consequently, the BLSS is a fully customizable platform for patient- and level-specific spinal implants. Although the present study focuses on fiber architecture for achieving tunable stiffness, the role of the matrix requires further investigation. Moreover, the mechanical behavior in this study was carried out under in vitro conditions and could not fully replicate the complex physiological environment experienced by natural ligaments, including hydration, temperature, and biochemical interactions. These factors affect ligament mechanics and long-term functional performance. Therefore, the incorporate matrix–fiber coupled will be designed, and the mechanical behavior under the physiologically relevant testing conditions will be evaluated in the future work.

## 4 | Experimental Section

### 4.1 | Design and Fabrication of Bioinspired Vertebrae

In this study, lumbar spine image data of a healthy male subject (24 years old, 178 cm, 74 kg) were obtained using CT (Brilliance iCT, Philips, The Netherlands) systems. A smoothed 3D model of the L3–L5 segments was reconstructed using Mimics (Materialize, Belgium) and Geomagic Wrap (3D Systems, American) software. Subsequently, 3D physical models of the L3–L5 vertebrae and natural IVDs were generated by CATIA (Dassault Systèmes, France). To enable integration with the BFLs, several holes were designed at the ligament attachment sites of the L3–L5 vertebrae based on anatomical morphology, facilitating stable fixation of the BFLs. The finalized bioinspired vertebra models were exported in .stl format and sliced in PreForm software (Formlabs Inc., USA). The bioinspired vertebrae were fabricated using a Formlabs Form 3D printer, which employs a precision laser to selectively cure liquid photopolymer resin layer by layer. Printing parameters, including layer thickness and support structures, were optimized to preserve anatomical fidelity and dimensional accuracy. Following fabrication, the printed vertebrae underwent standard postprocessing procedures, including rinsing in isopropyl alcohol and removal of support structures, to ensure mechanical strength and structural stability.

### 4.2 | Design and Fabrication of Bioinspired IVDs

Based on the function–structure characteristics of natural IVD, a bioinspired IVD model was established using SolidWorks software (Dassault Systèmes, France). The model consisted of a central bioinspired nucleus pulposus (NP), which occupies approximately 40% of the total cross-sectional area and is composed of isotropic material, and a peripheral bioinspired annulus fibrosus (AF). The AF was designed with three layers, each comprising alternating fibers and matrix layers. The fibers were orientated at an angle of 45°, and the stiffness of the matrix was designed to gradually increase from the inner to the outer layers. Bioinspired IVD model was exported in .stp format and imported into GrabCAD Print software (Stratasys Ltd., USA). Material properties were assigned according to the design specifications and the model was subsequently fabricated using 3D printing.

### 4.3 | Tensile Testing of BFLs

The mechanical performance of BFLs with different structural configurations was evaluated using a universal testing machine (UTM5504, SUNS, China) with a maximum load capacity of 30 000 N. Tests were carried out in displacement-control mode with a loading rate of 2 mm/min under cyclic tensile loading for 10 cycles and were terminated when the applied force reached 200 N. Throughout the experiments, force–displacement data were continuously recorded to evaluate the mechanical performance of BFLs.

### 4.4 | ROM Testing of BLSS

To assess the motion performance of the developed BLSS, a robotic testing platform was constructed. The platform consisted of a robotic arm (KUKA LBR iiwa 14 R820, KUKA, Germany), the BLSS, a six-axis force/torque sensor (LH–SZ–6W, Shanghai Liheng Sensor Technology Co., Ltd., China), and connecting components. The robotic arm was programmed to apply physiological 3D spinal motions. Subsequently, the ROM of the BLSS was measured and compared to evaluate its mechanical functionality.

### 4.5 | Fatigue Testing of BLSS

The compression–compression fatigue testing of the developed BLSS assembled by Method III was carried out by reference of ASTM F2346-05 in stress ration $R = -1$. The sinusoidal wave with the cyclic load of 400 N similar to that natural IVDs was applied by a fatigue testing system (TA Instruments ElectroForce 3300 Series, Water Technology Co., Ltd., USA); a frequency of 1 Hz was performed in air at room temperature (approximately 23°C and 40% relative humidity) with 100 000 cycles.

#### Author Contributions

**Guangsheng Song**: software (equal), methodology (equal), investigation (equal), data curation (lead), formal analysis (equal), validation (lead), visualization (lead), writing – original draft (lead), funding acquisition (supporting). **Weilong Jin**: software (equal); methodology (equal), investigation (equal), formal analysis (equal), visualization (supporting). **Guanghui Li**: investigation (supporting). **Yushan Sun**: methodology (supporting), investigation (supporting). **Jianan Wu**: investigation (supporting). **Hounan Song**: investigation (supporting). **Yuyang Wei**: investigation (supporting), formal analysis (supporting). **Kaize Wang**: investigation (supporting). **Zhende Jiang**: investigation (supporting). **Zhihui Qian**: methodology (supporting), conceptualization (lead), formal analysis (supporting), writing – review and editing (lead), funding acquisition (supporting). **Lei Ren**: visualization (supporting), supervision (supporting), funding acquisition (supporting). **Luquan Ren**: supervision (supporting).

#### Acknowledgments

The authors acknowledge the funding from the National Natural Science Foundation of China (grant nos. 52575334, U25A601, and 52405312), the Project from the Key Research and Development Program of Shandong Province (grant no. 2022CXPT043), and the China Postdoctoral Science Foundation Funded Project (grant nos. GZC20240589 and 2024M761111). The authors also acknowledge the Ethics Committee of the Second Hospital of Jilin University and all participants who written informed consents (grant no. 2021003).

#### Funding

This work was supported by the Project of the National Natural Science Foundation of China (No. 52575334, No. U25A601, No. 52405312), the Project of the Key Research and Development Program of Shandong Province (No. 2022CXPT043), and China Postdoctoral Science Foundation Funded Project (No. GZC20240589, No. 2024M761111).

#### Conflicts of Interest

The authors declare no conflicts of interest.

#### Data Availability Statement

All data needed to evaluate the conclusions are presented in the paper or requested from the corresponding authors.

#### References

1. F. Balagué, A. F. Mannion, F. Pellisé, and C. Cedraschi, "Non-Specific Low Back Pain," *Lancet* 379 (2012): 482–491.

2. B. I. Martin, R. A. Deyo, S. K. Mirza, et al., "Expenditures and Health Status among Adults with Back and Neck Problems," *JAMA* 299 (2008): 656–664.

3. K. Barri, Q. Zhang, I. Swink, et al., "Patient-Specific Self-Powered Metamaterial Implants for Detecting Bone Healing Progress," *Advanced Functional Materials* 32 (2022): 2203533.

4. G. Song, Z. Qian, K. Wang, et al., "Total Disc Replacement Devices: Structure, Material, Fabrication, and Properties," *Progress in Materials Science* 140 (2023): pp. 101189.

5. K. S. Emanuel, A. J. van der Veen, C. M. E. Rustenburg, T. H. Smit, and I. Kingma, "Osmosis and Viscoelasticity Both Contribute to Time-Dependent Behaviour of the Intervertebral Disc under Compressive Load: A Caprine In Vitro Study," *Journal of Biomechanics* 70 (2018): 10–15.

6. H. J. Wilke, L. Claes, H. Schmitt, and S. Wolf, "A Universal Spine Tester for In Vitro Experiments with Muscle Force Simulation," *European Spine Journal* 3 (1994): 91–97.

7. J. Choi, D. A. Shin, and S. Kim, "Finite Element Analysis of a Ball-and-Socket Artificial Disc Design to Suppress Excessive Loading on Facet Joints: A Comparative Study with ProDisc," *International Journal for Numerical Methods in Biomedical Engineering* 35 (2019): e3214.

8. J. Noailly, D. Lacroix, and J. A. Planell, "Finite Element Study of a Novel Intervertebral Disc Substitute," *Spine* 30 (2005): 2257–2264.

9. T. M. Grupp, J. J. Yue, R. Garcia, et al., "Evaluation of Impingement Behaviour in Lumbar Spinal Disc Arthroplasty," *European Spine Journal* 24 (2015): 2033–2046.

10. M. A. Bohl, S. McBryan, A. G. U. S. Newcomb, et al., "Range of Motion Testing of a Novel 3D-Printed Synthetic Spine Model," *Global Spine Journal* 10 (2020): 419–424.

11. S. T. Dukkipati and M. Driscoll, "Design Improvements and Validation of a Novel Fully 3D Printed Analogue Lumbar Spine Motion Segment," *Journal of Bionic Engineering* 21 (2024): 1388–1396.

12. K. Matsukawa, E. Taguchi, Y. Yato, et al., "Evaluation of the Fixation Strength of Pedicle Screws Using Cortical Bone Trajectory: What Is the Ideal Trajectory for Optimal Fixation?," *Spine* 40 (2015): E873–E878.

13. N. Sunni, G. N. Askin, R. D. Labrom, M. T. Izatt, M. J. Pearcy, and C. J. Adam, "The Effect of Repeated Loading and Freeze-thaw Cycling on Immature Bovine Thoracic Motion Segment Stiffness," *Proceedings of the Institution of Mechanical Engineers, Part H: Journal of Engineering in Medicine* 228 (2014): 1100–1107.

14. T. Belytschko, R. F. Kulak, A. B. Schultz, and J. O. Galante, "Finite Element Stress Analysis of an Intervertebral Disc," *Journal of Biomechanics* 7 (1974): 277–285.

15. Y. B. Guan, N. Yoganandan, J. Y. Zhang, et al., "Validation of a Clinical Finite Element Model of the Human Lumbosacral Spine," *Medical and Biological Engineering and Computing* 44 (2006): 633–641.

16. M. Xu, J. Yang, I. H. Lieberman, and R. Haddas, "Lumbar Spine Finite Element Model for Healthy Subjects: Development and Validation," *Computer Methods in Biomechanics and Biomedical Engineering* 20 (2017): 1–15.

17. G. Song, Z. Qian, X. Liu, et al., "Bioinspired Intervertebral Disc with Multidirectional Stiffness Prepared via Multimaterial Additive Manufacturing," *Advanced Functional Materials* 33 (2023): 2300298.

18. M. A. Bohl, M. A. Mooney, G. J. Repp, et al., "The Barrow Biomimetic Spine: Fluoroscopic Analysis of a Synthetic Spine Model Made of Variable 3D-Printed Materials and Print Parameters," *Spine* 43 (2018): E1368–E1375.

19. A. M. Levine and C. C. Edwards, "Traumatic Lesions of the Occipitoatlantoaxial Complex," *Clinical Orthopaedics and Related Research* 239 (1989): 53–68.

20. E. Gracey, A. Burssens, I. Cambre, et al., "Tendon and Ligament Mechanical Loading in the Pathogenesis of Inflammatory Arthritis," *Nature Reviews Rheumatology* 16 (2020): 193–207.

21. V. Musahl and J. Karlsson, "Anterior Cruciate Ligament Tear," *New England Journal of Medicine* 380 (2019): 2341–2348.

22. G. R. S. Naveh, J. E. Foster, T. M. S. Santisteban, X. R. Yang, and B. R. Olsen, "Nonuniformity in Ligaments Is a Structural Strategy for Optimizing Functionality," *Proceedings of the National Academy of Sciences* 115 (2018): 9008–9013.

23. K. L. Moffat, W.-H. S. Sun, P. E. Pena, et al., "Characterization of the Structure–function Relationship at the Ligament-to-Bone Interface," *Proceedings of the National Academy of Sciences* 105 (2008): 7947–7952.

24. D. Nepal, S. Kang, K. M. Adstedt, et al., "Hierarchically Structured Bioinspired Nanocomposites," *Nature Materials* 22 (2023): 18–35.

25. C. F. Ding, Y. K. Jin, Y. Y. Lin, et al., "Thermal Diode-Like Metafabric with Tunable Asymmetric Structure for Continuous Personal Cooling," *Materials Today* 85 (2025): 91–99.

26. Y. Gao, B. Xu, M. Qiu, et al., "Fabric-Reinforced Functional Insoles with Superior Durability and Antifracture Properties for Energy Harvesting and AI-Empowered Motion Monitoring," *Advanced Functional Materials* 35 (2025): 2416577.

27. M. Kanik, S. Orguc, G. Varnavides, et al., "Strain-Programmable Fiber-Based Artificial Muscle," *Science* 365 (2019): 145–150.

28. M. Li, L. Chen, Y. Li, et al., "Superstretchable, yet Stiff, Fatigue-Resistant Ligament-Like Elastomers," *Nature Communications* 13 (2022): 2279.

29. C. Y. Chen, L. J. Chen, Z. Y. Wu, et al., "3D Double-Faced Interlock Fabric Triboelectric Nanogenerator for Bio-Motion Energy Harvesting and As Self-Powered Stretching and 3D Tactile Sensors," *Materials Today* 32 (2020): 84–93.

30. Y. F. Wang, L. C. Li, D. Hofmann, J. E. Andrade, and C. Daraio, "Structured Fabrics with Tunable Mechanical Properties," *Nature* 596 (2021): 238–243.

31. C. Lu, X. Huang, H. Yan, et al., "Biomimetic Design of 3D Fibrous Mesh Reinforced Hydrogel Replicating the Form and Function of the Intervertebral Disc," *Small Structures* 4 (2023): 2200254.

32. E. Peña, J. A. Peña, and M. Doblaré, "On Modelling Nonlinear Viscoelastic Effects in Ligaments," *Journal of Biomechanics* 41 (2008): 2659–2666.

33. P. C. Hsu, A. Y. Song, P. B. Catrysse, et al., "Radiative Human Body Cooling by Nanoporous Polyethylene Textile," *Science* 353 (2016): 1019–1023.

34. S. Naserkhaki, N. Arjmand, A. Shirazi-Adl, F. Farahmand, and M. El-Rich, "Effects of Eight Different Ligament Property Datasets on Biomechanics of a Lumbar L4-L5 Finite Element Model," *Journal of Biomechanics* 70 (2018): 33–42.

35. Z. Xiao, L. Wang, H. Gong, D. Zhu, and X. Zhang, "A Non-Linear Finite Element Model of Human L4-L5 Lumbar Spinal Segment with Three-Dimensional Solid Element Ligaments," *Theoretical and Applied Mechanics Letters* 1 (2011): 064001.

36. M. A. Meyers, J. McKittrick, and P. Y. Chen, "Structural Biological Materials: Critical Mechanics-Materials Connections," *Science* 339 (2013): 773–779.

37. Z. Quan, A. Wu, M. Keefe, et al., "Additive Manufacturing of Multi-Directional Preforms for Composites: Opportunities and Challenges," *Materials Today* 18 (2015): 503–512.

38. G. Liu, X. Zhang, X. Chen, et al., "Additive Manufacturing of Structural Materials," *Materials Science and Engineering: R: Reports* 145 (2021): 100596.

39. B. K. Bhunia, D. L. Kaplan, and B. B. Mandal, "Silk-Based Multilayered Angle-Ply Annulus Fibrosus Construct to Recapitulate Form and Function of the Intervertebral Disc," *Proceedings of the National Academy of Sciences* 115 (2018): 477–482.

40. W. Fan, Z. Qian, G. Song, et al., "Fiber-Dependent 3D Anisotropic Stiffness-Tunable Biomimetic Intervertebral Disc via Multi-Material Additive Manufacturing," *Advanced Functional Materials* 35 (2024): 2414275.

41. S. J. Guo, J. Yang, G. Qiao, and X. S. Mei, "Assembly Deviation Modelling to Predict and Trace the Geometric Accuracy of the Precision Motion System of a CNC Machine Tool," *Mechanism and Machine Theory* 169 (2022): 104687.

42. E. Komendera and N. Correll, "Precise Assembly of 3D Truss Structures Using MLE-Based Error Prediction and Correction," *The International Journal of Robotics Research* 34 (2015): 1622–1644.

43. V. Lafage, N. Gangnet, J. Sénégas, F. Lavaste, and W. Skalli, "New Interspinous Implant Evaluation Using an Biomechanical Study Combined with a Finite-Element Analysis," *Spine* 32 (2007): 1706–1713.

44. M. M. Panjabi, T. R. Oxland, I. Yamamoto, and J. J. Crisco, "Mechanical Behavior of the Human Lumbar and Lumbosacral Spine As Shown by Three-Dimensional Load-Displacement Curves," *JBJS* 76 (1994): 413–424.

45. P. W. Hitchon, K. Eichholz, C. Barry, et al., "Biomechanical Studies of an Artificial Disc Implant in the Human Cadaveric Spine," *Spine* 2 (2005): 339–343.

46. F. Heuer, H. Schmidt, Z. Klezl, L. Claes, and H. J. Wilke, "Stepwise Reduction of Functional Spinal Structures Increase Range of Motion and Change Lordosis Angle," *Journal of Biomechanics* 40 (2007): 271–280.

47. H. J. Wilke, H. Schmidt, K. Werner, W. Schmölz, and J. Drumm, "Biomechanical Evaluation of a New Total Posterior-Element Replacement System," *Spine* 31 (2006): 2790–2796.

48. M. Y. Khalid, Z. U. Arif, A. Tariq, M. Hossain, R. Umer, and M. Bodaghi, "3D Printing of Active Mechanical Metamaterials: A Critical Review," *Materials & Design* 246 (2024): 113305.

## Supporting Information

Additional supporting information can be found online in the Supporting Information section. **Supporting Fig. S1:** Tensile testing of BFLs. (a) Universal testing machine (UTM5504, SUNS, China) and tensile testing of the developed BFLs. (b) Tensile testing conditions. **Supporting Fig. S2:** Stiffness in toe region of BFLs compared to reported cadaveric data [1, 2]. (a) Stiffness in toe region of B-ALL in comparison with the cadaveric data. (b) Stiffness in toe region of B-PLL in comparison with the cadaveric data. (c) Stiffness in toe region of B-ISL in comparison with the cadaveric data. (d) Stiffness in toe region of B-SSL in comparison with the cadaveric data. (e) Stiffness in toe region of B-LF in comparison with the cadaveric data. (f) Stiffness in toe region of B-ITL in comparison with the cadaveric data. The results were showed

with mean ± standard deviation (SD). **Supporting Fig. S3:** 3D model of the L3-L5 segment was established based on human CT images. (a) CT scans of healthy subjects. (b) CT image. (c) CT image segmentation. (d) Bioinspired vertebrae and IVD models. **Supporting Fig. S4:** Geometric design and preparation process of bioinspired vertebrae. (a) Front view. (b) Rear view. (c) Side view. (d) The preparation process of the bioinspired vertebra sample by 3D printing technology. The structural parameters were listed in Table S1. To fix the developed BFLs, M5 holes were designed in the vertebrae body and M2 threaded holes were designed in the vertebrae arch. **Supporting Fig. S5:** Geometric parameters of bioinspired IVD in L3-L4 segment. (a) Structural parameter of the bioinspired NP. (b) Structural parameters of each AF layer thickness. (c) Dimensional parameters of the AF layer numbers. (d) Structural parameters of the AF fibers. (e) External dimensions of the bioinspired IVD in L3-L4 segment. (f) Height dimensions of the bioinspired IVD in L3-L4 segment. The structural parameters were listed in Table S2. **Supporting Fig. S6:** Geometric parameters of bioinspired IVD in L4-L5 segment. (a) Structural parameter of the bioinspired NP. (b) Structural parameters of each AF layer thickness. (c) Dimensional parameters of the AF layer numbers. (d) Structural parameters of the AF fibers. (e) External dimensions of the bioinspired IVD in L4-L5 segment. (f) Height dimensions of the bioinspired IVD in L4-L5 segment. The structural parameters were listed in Table S3. **Supporting Fig. S7:** Testing blocks. (a) The upper testing block is connected to the L3 vertebra. (b) The lower testing block is connected to the L5 vertebra. The upper curved surface configuration matches the L3 vertebra and L5 vertebra, respectively. They are fixed to each other using a superglue (Epoxy resin adhesive, UHU, Germany). **Supporting Fig. S8:** The ROM testing of BLSS. Experimental setup for the ROM testing, showing the BLSS integrated with a multi-axis motion platform. The ROM data was collected and analyzed under different loading condition, illustrating the developed BLSS functionality to replicate physiological spinal kinematics. **Supporting Fig. S9:** Fatigue testing of BLSS assembled by method III. (a) Fatigue testing platform. (b) Height deformation after 100,000 loading cycles. (c) The applied peak load value after 100,000 loading cycles. (d) The ROM results before and after fatigue in compression mode. This comparison showed that the ROM hardly changed before and after fatigue, further demonstrating that BLSS had long-term mechanical stability. **Supporting Table S1:** Structural parameters of bioinspired vertebrae model. **Supporting Table S2:** Structural parameters of bioinspired IVD model in L3-L4 segment. **Supporting Table S3:** Structural parameters of bioinspired IVD model in L4-L5 segment.